Forest Biomass Mapping Using Continuous InSAR and Discrete Waveform Lidar Measurements: A TanDEM-X/GEDI Test Study

Changhyun Choi, Matteo Pardini, *Member, IEEE*, John Armston, and Konstantinos P. Papathanassiou, *Fellow, IEEE*

***Abstract*—This article addresses the implementation of an above ground biomass (AGB) estimation scheme relying on the height-to-biomass allometry at stand level in the context of the synergistic use of continuous TanDEM-X (bistatic) interferometric synthetic aperture radar acquisitions and spatial discrete GEDI waveform lidar measurements. The estimation of forest height and horizontal forest structure from TanDEM-X data in the absence of a digital terrain model (DTM) is discussed. The possibility of estimating (top) canopy height variations independent of topographic height variations is discussed using wavelet-based scale analysis. This understanding is then exploited to define a structure index expressing the (top) canopy-only height variations in the absence of a DTM. The potential of using the derived structure information to account for the spatial variability of height-to-biomass allometry derived from the GEDI measurements is addressed. The performance of the conventional height-to-biomass allometry and the one achieved by the locally adapted implementation are compared against reference lidar measurements and discussed. The analysis is carried out using GEDI and TanDEM-X interferometric measurements and validated by using LVIS lidar measurements over the Lopé National Park, a diverse tropical forest test site in Gabon.**

***Index Terms*—Above ground biomass (AGB), forest height, forest structure, GEDI, synthetic aperture radar (SAR), SAR interferometry, tandem-x, waveform lidar.**

I. Introduction

THE potential of spaceborne LiDAR or interferometric synthetic aperture radar (InSAR) configurations to measure forest height at spatial scales of about or below 1 hectare (ha) motivates the use of the so-called forest height-to-biomass allometry at stand level. Accordingly, the above ground biomass (AGB) B of a stand is expressed in terms of an exponential allometric relationship as a function of its top canopy height H [1], [2], [3], [4], [5]

$$\mathrm{B} = \alpha_0 \cdot \mathrm{H}^{\beta_0} \tag{1}$$

where α_0 is the allometric level and β_0 the allometric exponent. The allometric exponent β_0 defines the underlying allometric relationship defined by species composition, growth conditions, and development stage. The allometric level α_0 accounts for anthropogenic or natural variations in stand density resulting from differences in basal area, age composition, thinning operations, and/or different disturbance effects.

Obviously, any practical application of (1) requires knowledge of the two allometric parameters α_0 and β_0 and of their spatial variability in addition to accurate measurements of top canopy height. And while the allometric exponent can remain constant over larger scales, the allometric level may vary locally at much smaller scales.

This article addresses the implementation of an AGB estimation scheme relying on a stand-level height-to-biomass allometry as defined in (1), in the context of a synergistic combination of data provided by two different Earth observation missions: the DLR's InSAR TanDEM-X mission [6] and the NASA's waveform Lidar GEDI mission [7]. GEDI samples forest structure by means of lidar waveforms in a more or less dense grid and provides forest height measurements and a set of waveform metrics that allow to estimate AGB [7], [8]. Complementarily, TanDEM-X provides a continuous high spatial resolution InSAR data set with inherent sensitivity to (vertical) forest structure. In the context of (1), spatially continuous forest height estimates derived from the interferometric TanDEM-X data can be used to obtain spatially continuous AGB estimates as long as (α_0, β_0) are known. While the GEDI forest height and biomass measurements can be used to estimate the allometric exponent β_0 and to define the general height-to-biomass allometry at regional or even finer scales, they may be not able to derive the faster varying allometric level α_0. The question is therefore if, and if so, how accurate the spatial variability of α_0 can be derived (or tracked) from TanDEM-X InSAR data.

Indeed, the partial or even complete reconstruction of the 3D radar reflectivity from InSAR or tomographic SAR data and the derivation of a number of (more or less physical) structure indices related to the horizontal and/or vertical forest structure have been demonstrated in several studies [9], [10], [11], [12], [13], [14], [15], [16], [17], [18]. In [18], a horizontal forest

Manuscript received 30 July 2022; revised 14 June 2023 and 24 July 2023; accepted 25 July 2023. Date of publication 4 August 2023; date of current version 25 August 2023. This work was supported by NASA under Grant #80NSSC20K0023 to the University of Maryland in the frame of a joint research project between DLR and NASA's Carbon Monitoring System (CMS) Program. *(Corresponding author: Changhyun Choi.)*

Changhyun Choi, Matteo Pardini, and Konstantinos P. Papathanassiou are with the Microwave Institute, Deutsches Zentrum fur Luft- und Raumfahrt Standort Oberpfaffenhofen, 82234 Wessling, Germany (e-mail: cch947@gmail.com; matteo.pardini@dlr.de; kostas.papathanassiou@dlr.de).

John Armston is with the Department of Geographical Sciences, University of Maryland at College Park, College Park, MD 20742 USA (e-mail: armston@umd.edu).

Digital Object Identifier 10.1109/JSTARS.2023.3302026

structure index HS derived from InSAR TanDEM-X data has been successfully used to account for the spatial variability of the allometric level in heterogeneous forests

$$\mathrm{B} = \alpha\,(\mathrm{HS}) \cdot \mathrm{H}^{\beta_0} \tag{2}$$

and to improve biomass estimation performance. HS quantifies the height variability of the top canopy "surface." An increase in HS indicates a more heterogeneous canopy surface in the horizontal direction and is interpreted as a sparser forest stand. There are two arguments in favor of using HS: its close correlation with the well-established stand density index [19] and thus with basal area [16] and the fact that it can be derived from InSAR TanDEM-X data. However, the estimation of HS in [18] requires the availability of a digital terrain model (DTM). The lack of appropriate DTMs for most of the forested regions limits the application of (2) for biomass estimation.

In this article, the relationship in (2) is applied to a very general case where only a single polarisation TanDEM-X interferogram and a set of spatially discrete GEDI waveform measurements are available, but no DTM is provided. The intention is to develop a methodologic concept under the perspective of forest biomass inversion on a large scale rather than discussing the optimization of performance on a local scale.

Forest height is derived from TanDEM-X data. Many different ways to invert forest height from TanDEM-X data have been discussed in the literature [20], [21], [22], [23], [24]. In the case of TanDEM-X data acquired in the global digital elevation model (DEM) mode [6], the availability of a single polarisation interferogram allows only a highly simplified inversion implementation. This can be only done on the basis of very simplified inversion models, which often need to be supported by additional information, e.g., by using parameters derived from lidar measurements and/or an external DTM [24], [25]. Here, the methodology proposed in [24] and [25] which inverts height from TanDEM-X interferometric coherence using the available GEDI waveforms has been used. The advantage of the proposed approach is that it allows unbiased height estimates over large scales in the absence of a DTM. The price for this is a high(er) variance when compared to other approaches.

The allometric level α_0 and exponent β_0 are derived from the GEDI footprint measurements. The dependency of the allometric level on the forest structure index $\alpha(\mathrm{HS})$ is no longer possible to be established in the absence of a DTM in the context of [18]. Instead of using a DTM for removing the topographic variation in the estimation of HS, the low-pass filtered TanDEM-X DEM is used. Even though this approach is well established in interferometric data processing, here it has to be evaluated to what extent and on which spatial scales the phase variations induced by the terrain can be separated from the phase variations induced by the vegetation and to what extent it affects the performance of the HS estimation.

The rest of this article is organized as follows. Section II describes the selected forest site for the experiments, i.e., the Lopé National Park in Gabon, the experimental data (TanDEM-X and GEDI), and the reference height and biomass measurements available. Section III addresses the estimation of a horizontal structure index from TanDEM-X data in the absence of a DTM. In Section IV, the forest height estimation from TanDEM-X data is reviewed. The use of the derived horizontal structure information to improve forest height estimation performance is proposed. Section V addresses the derivation of the forest height-to-biomass allometry from the GEDI measurements. In Section VI, the biomass estimation using the height, structure, and GEDI derived height-to-biomass relations is performed and assessed. Finally, Section VII, concludes this article.

II. Test Sites and Data Sets

The experiments in this study focus on an area within the Lopé National Park in Gabon covered during the AfriSAR campaign in 2016 [26], [27]. The site consists of a variety of forest structure types ranging from open savannas to undisturbed tall (sometimes exceeding 50 m) and dense forest stands. Colonizing forest (sparse forest stands mixed up with savanna) or monodominant Okoume (dense, mono-layered, tall, and dense forest stands) are two particular cases [28], [29], [30], [31], [32]. Biomass ranges between around 10 t/ha in savanna areas and ∼600 t/ha in the dense forest areas. The terrain is hilly with many local slopes steeper than 20°. The available lidar and radar data are described in the following and summarized with their resolution in Tables I and II.

Lidar full-waveform data were collected by NASA's Land and Vegetation and Ice Sensor (LVIS) in February 2016 [27]. LVIS footprints have a mean diameter of about 22 m and overlap partially on ground [27]. At each footprint, the RH100 (the height above ground at which 100% of the full-waveform energy is cumulated) is estimated from the waveform. The RH100 heights have been projected in geographic UTM coordinates and resampled at a 20 m grid. These resampled RH100 heights, denoted in the following as $\mathrm{H_{LVIS}}$, are shown in Fig. 1(a) and are used as a reference for the validation of the TanDEM-X height estimates. The reference LVIS heights $\mathrm{H_{LVIS}}$ are further averaged to a 50 m × 50 m and a 100 m × 100 m resolution. The obtained heights are referred as $\mathrm{H_{LVIS50}}$ and $\mathrm{H_{LVIS100}}$, respectively. Furthermore, two AGB maps at 50 m × 50 m (referred as $\mathrm{B_{LVIS50}}$) and 100 m × 100 m (referred as $\mathrm{B_{LVIS100}}$) resolution, both estimated from the LVIS waveforms, are used as biomass reference. These AGB maps have been obtained by means of a relationship formally equivalent to the one in (2). The RH98 is used to calculate the top forest height, while RH90, canopy cover, and regional values of wood specific gravity are used to calculate the allometric level. The relationships are further parameterized by using the field inventory plots [28], [29]. The DTM and the canopy height model (CHM) resampled at 1 m × 1 m resolution have been used as well. Both of them were derived from small-footprint (10 cm) discrete-return lidar data acquired in July 2015 covering part of the Lopé site [32].

The TanDEM-X dataset was selected to be acquired close in time to the LVIS flights. The relevant acquisition parameters are summarized in Table II. The mean height of ambiguity (HoA) of about 65 m allows optimum forest height estimates in the range between 15 and 45 m [25], [33]. For shorter and taller heights, the forest height estimation performance is expected to be more or less compromised [33].

TABLE I
SUMMARY OF LIDAR DATA AND TANDEM-X PRODUCTS

Data	Product	Symbol / Acronym	Resolution	Grid sampling
Small-footprint lidar	DTM / digital canopy model	DTM/CHM	1 m × 1 m	1 m × 1 m
LVIS	RH100 at footprint level	H_{LVIS}	22 m (footprint diameter)	20 m × 20 m
	Mean RH100	H_{LVIS50}	50 m × 50 m	
		$H_{LVIS100}$	100 m × 100 m	
	Above ground biomass	B_{LVIS50}	50 m × 50 m	
		$B_{LVIS100}$	100 m × 100 m	
GEDI	Level 2A RH100	H_{GEDI}	25 m (footprint diameter)	
	Level 4A AGB	B_{GEDI}		
TanDEM-X	"Few-looks" phase center heights		5 m × 5 m	5 m × 5 m
	DEM	DEM	120 m × 120 m	
	Canopy height profiles (CHP)	CHP	25 m × 25 m	20 m × 20 m
	Top peak height	Z_{top}	25 m × 25 m	
	Horizontal structure index	σ_{top}	100 m × 100 m	
	Forest height	H_{TX}	25 m × 25 m	
		H_{TX100}	100 m × 100 m	
	Above ground biomass	AGB	100 m × 100 m	

TABLE II
SUMMARY OF TANDEM-X ACQUISITION PARAMETERS

Test Site	Lopé
Acquisition Date	Jan. 25, 2016
Frequency	X-band
Polarization	HH
Ground resolution (Range / Azimuth)	1.95 m / 1.99 m
Vert. wavenumber	~ 0.10 m^{-1}
HoA	~ 62.8 m
Incidence angle	~ 44.5°

The GEDI data over Lopé available for this study have been acquired in the first 18 months of the mission between April 2018 and October 2019. For each International Space Station pass, the three GEDI lasers collected data along eight tracks separated by about 600 m in the across-track direction. Along each track, waveforms with a footprint of approximately 25 m diameter are measured every 60 m. In Lopé, this results into 12 000 footprints distributed as shown in Fig. 1(b) corresponding to only 0.6% of the LVIS coverage. The GEDI waveforms, the Level 2A RH100 values (referred as H_{GEDI}) [34], as well as the derived Level 4A AGB values (referred as B_{GEDI}) [35] have been used to initialize the height estimation from TanDEM-X coherences and to define the height-to-biomass relationship(s).

III. HORIZONTAL STRUCTURE INDEX ESTIMATION

Originally, the estimation of the horizontal forest structure index was proposed either from tomographically reconstructed radar reflectivity profiles at L-band or from lidar waveforms [16], [17]. In [18], a similar—yet simplified—horizontal structure index has been derived from CHPs, i.e., the histograms of the InSAR "few-look" phase center heights [23], [36], [37] within a certain resolution cell. In particular, the variation of top canopy height reflected by the CHPs after the compensation of the terrain-induced (height) variations by using an available DTM was used to derive the horizontal structure index. However, in the absence of a DTM, this approach is not possible for sites with relevant topographic variations. To circumvent this rather serious limitation, the question of the existence of spatial scales at which top canopy height variations are independent or at least less affected by topographic height variations becomes important. This question is addressed in the section.

A. Wavelet Variance Analysis

To evaluate the effects of both top canopy and topographic height variations on the TanDEM-X InSAR few-look phase at different spatial scales, a wavelet decomposition analysis is employed, similar to the one proposed and performed in [10] and [38]. For this, the wavelet spectrum of the TanDEM-X few-look phase center heights (as obtained by dividing the unwrapped InSAR phase by the local terrain-corrected vertical wavenumber κ_z [33], [39]) are compared with the available CHM spectrum (representing the top canopy height variations) and the DTM

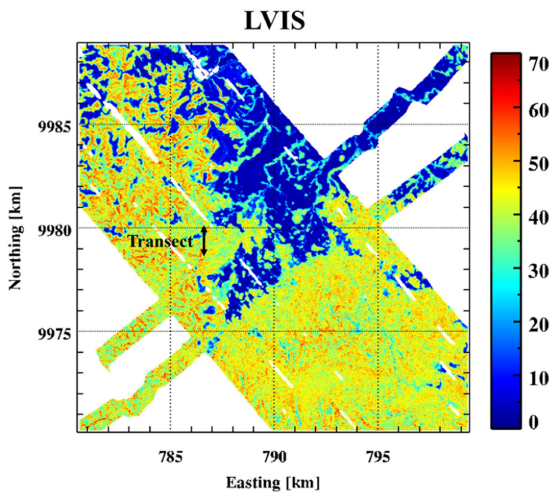

(a)

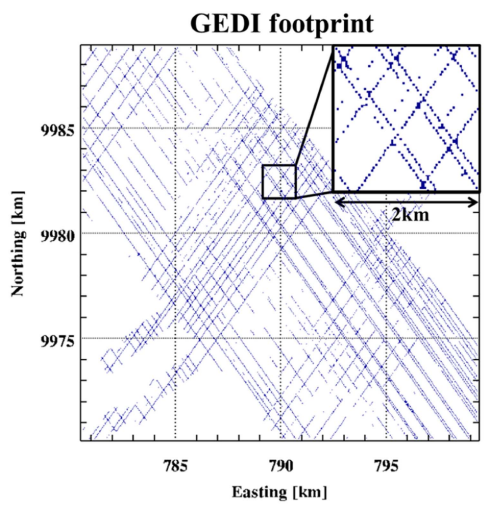

(b)

Fig. 1. Lopé site. (a) LVIS RH100 H_{LVIS} map in meters (m). (b) Footprint positions of the available GEDI measurements. Both maps are in UTM coordinates, with spacing (20 m × 20 m) in easting and northing direction, and they cover around 19 km by 19 km. The black line in (a) indicates a representative transect used for the wavelet analysis in Fig. 2.

spectrum (representing the topographic height variations), both derived from the small-footprint lidar data.

For the sake of simplicity, all the height maps were projected in geographic UTM coordinates and resampled on the same 1 m grid in both easting (x) and northing (y) directions. Before transforming to UTM, the TanDEM-X few-look phase center heights have been obtained from a multilooking operation with resolution 5 m × 5 m (corresponding to six independent looks, two in range, and three in azimuth) in order to reduce the phase variance induced by the interferometric decorrelation.

For each height map $f(x, y)$, the wavelet spectrum has been calculated as a function of the (horizontal) scale parameter s as [10], [38], [40]

$$WS_s = \langle c_{x,s}^2 + c_{y,s}^2 \rangle \tag{3}$$

where $\langle \cdot \rangle$ indicates a moving average operator within 100 × 100 m cells introduced to reduce local fluctuations. As

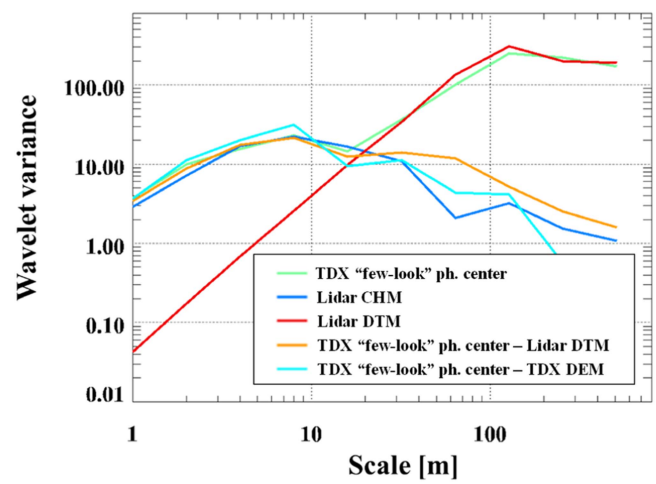

Fig. 2. Lopé site: wavelet variance WS as a function of the scale s for the small-footprint lidar heights (DTM and CHM) and TanDEM-X "few-look" phase center heights averaged along the representative transect shown in Fig. 1(a).

indicated by their subscripts, all quantities in (3) are 2D in (x, y) and depend on s, $c_{x,s}$ and $c_{y,s}$ are the coefficients along the x and y directions associated with the chosen 1D mother wavelet, respectively. Each value of s corresponds to a dilation of the mother wavelet, which is used to generate the impulse response of a filter. Its application to the input height maps along x and y provides $c_{x,s}$ and $c_{y,s}$ [38]. If the mother wavelet is a symmetric and odd function of the spatial variable, the corresponding filter resembles a differential operator producing a (mean) height difference between points at a distance corresponding to the scale [38], [40], i.e.,

$$\begin{aligned} \langle {c_{s,x}}^2 \rangle &\cong \left\langle [f(x + \Delta x, y) - f(x, y)]^2 \right\rangle \\ \langle {c_{s,y}}^2 \rangle &\cong \left\langle [f(x + \Delta y, y) - f(x, y)]^2 \right\rangle \end{aligned} \tag{4}$$

with Δx and Δy proportional to s. In this way, WS_s reflects directly 2D variations of the input heights as a function of s [10], [38]. For the wavelet decomposition, the PyWavelets Python package [41] has been used with the biorthogonal 1.3 function as the mother wavelet for a reliable approximation of (4).

Fig. 2 illustrates the behavior of the three (TanDEM-X few-look phase center heights, and lidar CHM and DTM) WS_s as a function of the scale parameter s averaged along a representative 7-km long north–south transect in Lopé [see Fig. 1(a)] covered by dense forest stands and with a significant topographic variation. The relative effect of top canopy and topographic height variations on the TanDEM-X few-look phase center height at the different spatial scales becomes clearly visible: while at smaller scales (up to 10 m), the TanDEM-X phase center height (green line) is highly correlated with the CHM (blue line) and widely independent of the DTM (red line), at larger scales (>30 m) it correlates with the DTM while its dependency on the CHM decreases fast with increasing scale.

The plot makes clear that the estimation of top canopy height variations (and consequently the estimation of the horizontal structure index) by means of the CHPs without compensating for the terrain-induced height variations is problematic at scales

larger than 30 m as both top canopy and terrain height variations are relevant. In order to reflect only the top canopy height variations, the TanDEM-X few-look phase center height variation should be estimated at a 10 m scale (or finer). This becomes difficult due to the phase center height (i.e., phase) variance induced by interferometric decorrelation.

To compensate for the effect of terrain variations, the TanDEM-X few-look phase center heights are corrected once by using the DTM and once with a low-pass filtered (up to a spatial resolution of 120 m) version of its own. The use of a low-pass filtered DEM for removing the topographic variation is an established technique in interferometric SAR processing [23], [37], [42], [43]. However, the question here is to find at what scale this is best possible and how much it compromises the HS estimation performance. The value of 120 m has been chosen with reference to the behavior of TanDEM-X phase center heights in Fig. 2: at this scale, the top canopy height variations are attenuated (with respect to its maximum) while the topographic ones are maximized. As expected, the DTM corrected TanDEM-X few-look phase center heights (orange line) in Fig. 2 follow closely the CHM behavior at all scales. The self-corrected TanDEM-X few-look phase center heights (cyan line) behave similarly and follow the CHM heights across the whole range of scales as well.

B. Structure Index Definition

Based on the analysis above, the horizontal structure estimation framework defined in [18] is now adapted to the self-corrected TanDEM-X few-look phase center heights. The CHPs are calculated as the histograms of the self-corrected heights, followed by smoothing with a Gaussian window of 3 m width. The zero height of each CHP is now a local reference height provided by the low-pass filtered TanDEM-X phase center heights. As the real ground height is unknown, the determination of the top layer in which the significant canopy height variations occur is not straightforward [18]. This requires the definition of a structure index by means of a relative height. For this, only the peak at the highest height with a value above threshold, called "top" peak in the following, of each CHP in a structure cell is retained in a set Z_{top}. The threshold is set at 10% of the absolute maximum value reached by each CHP. This thresholding operation, together with the histogram smoothing, aims at reducing the impact of using a small number of looks in the calculation of the phase center heights and to avoid the creation of insignificant peaks which may bias the structure quantification. The horizontal structure index employed here is defined as [44]

$$\sigma_{top} = \sqrt{\mathrm{var}\{Z_{top}\}} \tag{5}$$

where var$\{\cdot\}$ indicates the variance of the set. A high σ_{top} indicates large top canopy height variations (i.e., large canopy roughness) as in the case of a sparse forest, while a low σ_{top} indicates smaller variations (i.e., low canopy roughness) as in the case of a dense(r) forest. The use of the CHPs allows to maximize the sensitivity to the top canopy variations as it accounts only for the behavior of the "top" peak. Examples of CHPs for two relevant transects in dense and sparse forests are shown in Fig. 3,

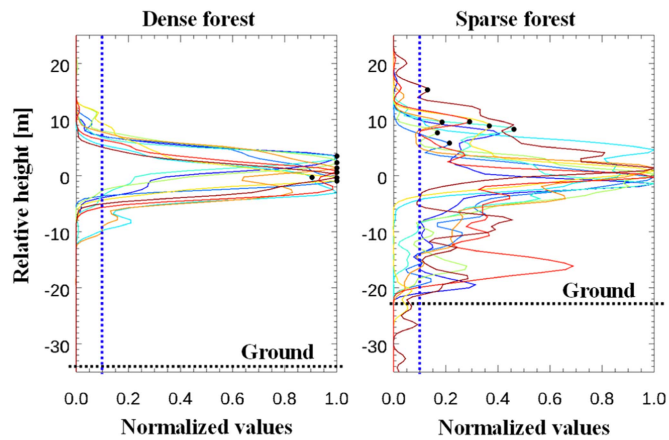

Fig. 3. Examples of consecutive CHPs extracted along two transects in dense and sparse forest stands (areas A and B in the following of the article). Each CHP corresponds to a 25 m × 25 m cell on ground. The zero of the vertical axis represents the low-pass filtered TanDEM-X DEM height in the location of each CHP. The average ground height is reported (horizontal black dashed lines). For each CHP, the peak at the maximum height with a value above the threshold indicated by the vertical blue dashed line is retained in Z_{top}. The extracted peaks are denoted with a black dot.

and the "top" peak is marked for each of them. It is apparent that in the sparse forest case, the "top" peak heights vary in a larger height interval than in the dense forest case, leading to a larger σ_{top}.

With reference to the spatial grid samplings and resolutions in Table I, σ_{top} is derived by means of (5) at 100 m resolution (i.e., for 100 my× 100 m structure cells) as follows.

1) The single look complex TanDEM-X phase center height is multilooked to 5 m × 5 m cells (6 looks).
2) The terrain-induced height variations are compensated by subtracting a low-pass filtered (to a spatial resolution of 120 m) version of its own.
3) The CHPs are calculated at 25 m resolution (i.e., 25 m × 25 m cells) from 25 phase center height samples and for each CHP Z_{top} is derived.
4) The variance of Z_{top} within a 100 m × 100 m structure cells, i.e., across 25 Z_{top} samples (equivalent to 16 independent samples), is estimated and used in (5) to calculate σ_{top}.

The obtained map of Fig. 4 shows sparse forest areas ($\sigma_{top} >$ 5 m) surrounded by denser ones ($\sigma_{top} <$ 5 m) in the southeastern part of the site, while they are distributed along the slopes in the northwestern one.

Although the proposed horizontal structural index is able to distinguish dense from sparse forest stands, even to some extent, σ_{top} becomes ambiguous at forest nonforest transitions, misinterpreting the step-like height change as increased top canopy variations, and often classifying the transition zone as sparse forest. Such border areas can be identified by using a forest/nonforest mask [45]. When forest and nonforest attributed samples are present within a 100 m σ_{top} estimation cell, the cell is set as a border area. In this way, the 3% of the forested area in the site is classified as a border area and excluded. In order to exclude an additional error factor from the interferometric

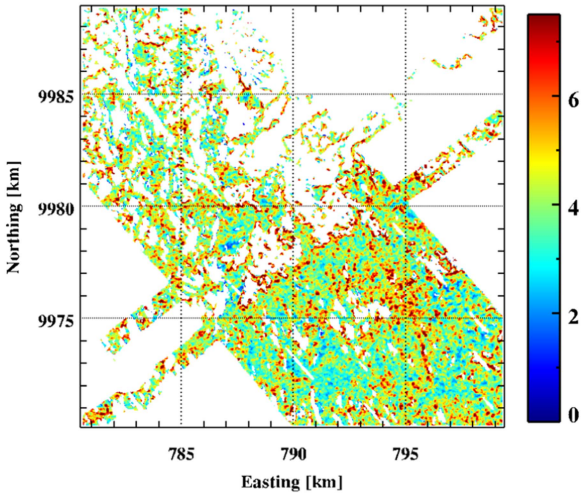

Fig. 4. Lopé site, same area as in Fig. 1. Map of σ_{top} at 100 m × 100 m resolution.

phase, hilly areas (i.e., slopes larger than 15°) corresponding to ∼10% of the forested area were masked as well, resulting in the exclusion of low coherence areas characterized by higher phase noise.

IV. Forest Height Estimation From TanDEM-X Coherence Magnitude

A. Methodology

For a bistatic single-polarization TanDEM-X acquisition, the InSAR complex coherence can be factorized as [39], [46]

$$\tilde{\gamma}\left(\kappa_z\right) = \gamma_{SNR} \cdot \gamma_{rg}\left(\kappa_z\right) \cdot \gamma_Q \cdot \tilde{\gamma}_V\left(\kappa_z\right) \tag{6}$$

where γ_{SNR} is the additive noise (SNR) decorrelation, $\gamma_{rg}(\kappa_z)$ is the range spectral decorrelation, and γ_Q is the quantization decorrelation. Forest height (H_V) is estimated from the volume decorrelation contribution $\gamma_V(\kappa_z)$

$$\tilde{\gamma}_V\left(\kappa_z\right) = \exp\left(i\kappa_z z_0\right) \frac{\int_0^{H_V} F\left(z\right) \exp\left(i\kappa_z z\right) dz}{\int_0^{H_V} F\left(z\right) dz} \tag{7}$$

where $F(z)$ is the vertical distribution of scatterers, H_V is the forest (top canopy) height [that defines the upper boundary of $F(z)$], and z_0 a reference height corresponding to the lower boundary of $F(z)$. κ_z is the vertical (interferometric) wavenumber defined for bistatic interferometers as

$$\kappa_z = \frac{2\pi}{\lambda} \frac{\Delta\theta}{\sin\left(\theta_0 - a\right)} \tag{8}$$

where λ is the wavelength, $\Delta\theta$ is the change of the incidence angle induced by the spatial baseline, θ_0 is the nominal incidence angle, and a is the range terrain slope. The terrain slopes can be obtained from an available DEM, and for this, the TanDEM-X DEM has been used.

Following the approach proposed in [25] the available GEDI waveforms are used to derive a "mean" vertical reflectivity profile over a whole TanDEM-X scene. For this, first, the so-called profile matrix $[P]$ is formed with columns of the GEDI waveforms $P_i(z)$ in the scene normalized to unit height (and resampled to a common number of height samples). Accordingly, the number of rows of $[P]$ is given by the number of height samples and the number of columns by the number of available GEDI waveforms. From the profile matrix, a covariance matrix $[R]$ is formed

$$[R] = [P]\ [P]^T \tag{9}$$

where $[\cdot]^T$ indicates the transpose operation, and then diagonalized

$$[R] = [U]\ [\Lambda]\ [U]^T \tag{10}$$

where $[\Lambda]$ contains the (positive) eigenvalues a_i and $[U]$ the eigenvectors $\bar{P}_i(z)$ of $[R]$. The eigenvectors $\bar{P}_i(z)$ of $[R]$ are then used to compose the mean reflectivity profile

$$P_{mean}\ (z) = \sum_{i=1}^{M} a_i \bar{P}_i\ (z) \tag{11}$$

where M represents the number of eigenvectors used to compose $P_{mean}(z)$. In the following, only the first eigenfunction

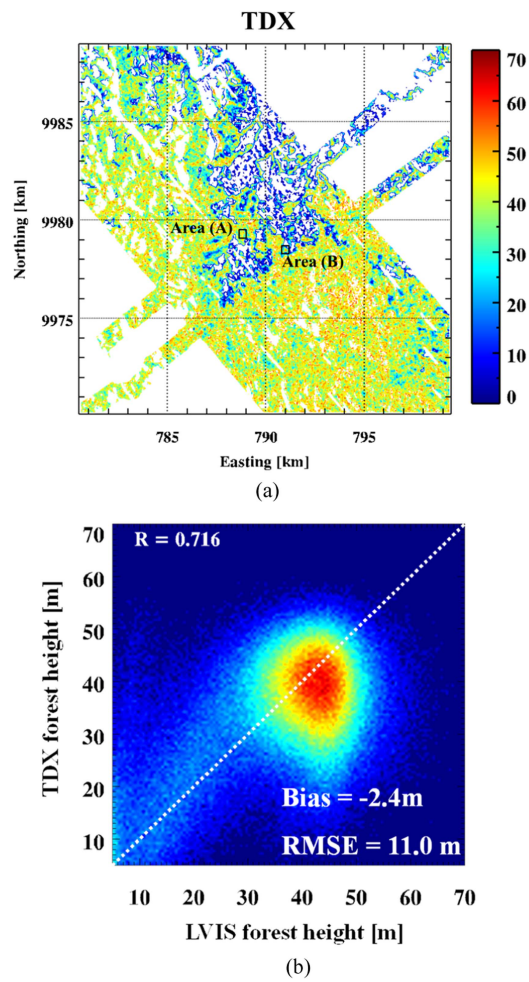

Fig. 5. Lopé site, same area as in Fig. 1. (a) TanDEM-X forest height H_{TX} in meters (m). (b) Comparison (2D histogram) between H_{TX} and H_{LVIS}. The height estimation performance in the areas (A) and (B) indicated in (a) is further investigated in Fig. 6.

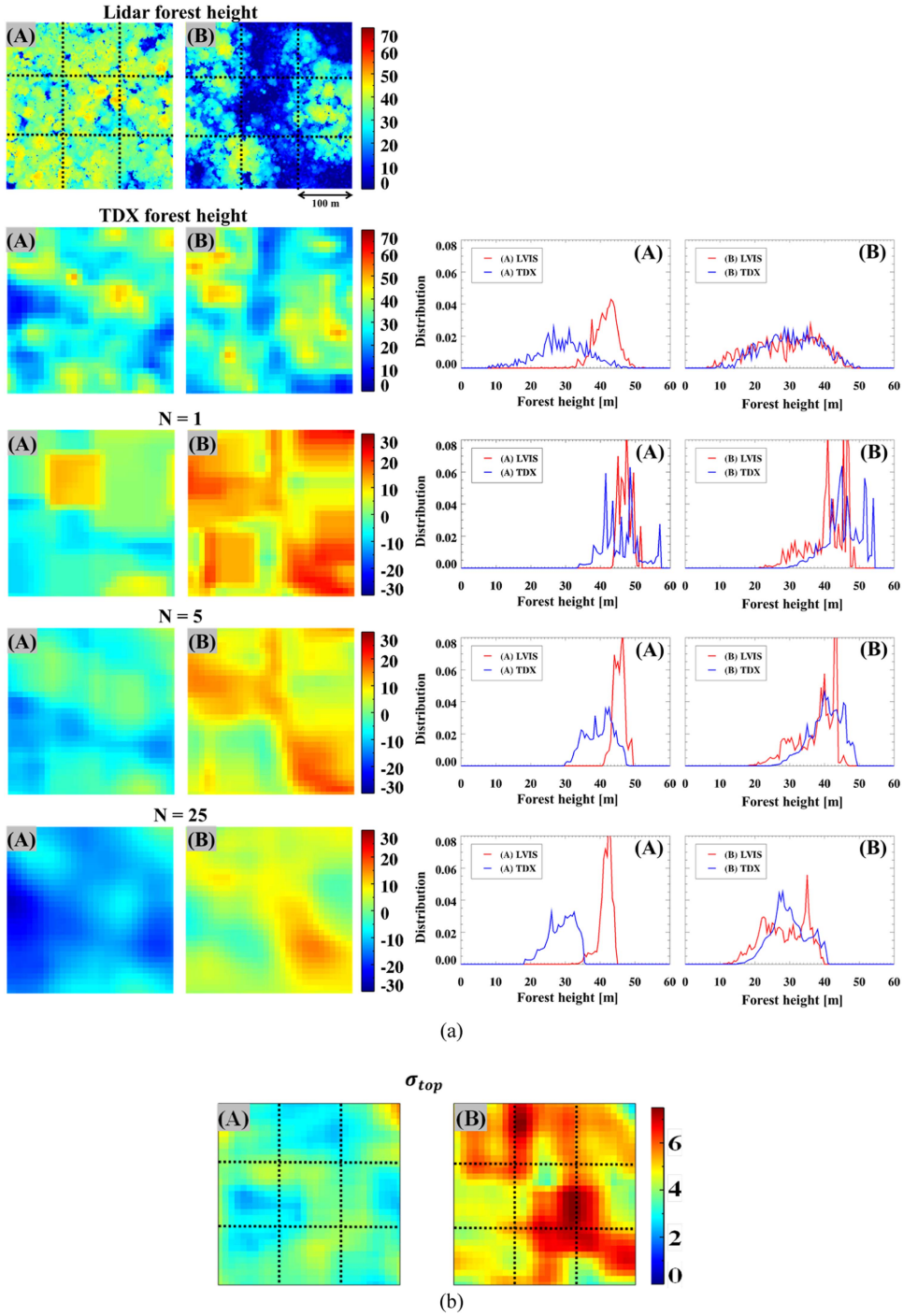

Fig. 6. Lopé site. (a) Height estimates and related errors for representative dense (area A) and sparse (area B) areas. The locations of areas A and B are illustrated in Fig. 5(a). First row: small-footprint lidar CHM. Second row: TanDEM-X H_{TX} (25 m resolution). Third, fourth, and fifth rows: height errors $H_{TX100} - H_{LVIS100}$ (100 m resolution) for $N = 1, 5, 25$, respectively, as in (12) on the left; and histograms of H_{TX} and H_{LVIS} (25 m resolution) on the right. (b) Maps of σ_{top} over areas A and B. In the maps in (a) and (b) the black dashed lines separate nonoverlapping height resolution cells measuring 100 m × 100 m.

$P_{mean}(z) = \bar{P}_1(z)$ has been used for defining the mean reflectivity profile. The low-frequency profile component given by the first eigenvector is more appropriate for describing forest reflectivity over larger spatial scales, since the higher order profile components may locally mismatch with the actual reflectivity due to the natural spatial heterogeneity of the forest structure. In terms of the achieved estimation performance, the low-frequency profile component is sufficient because the effect of the vertical reflectivity on the volume decorrelation is smaller compared to the effect of the forest height.

The use of the mean reflectivity profile $P_{mean}(z)$ instead of the vertical distribution of scatterers $F(z)$ in (7) leads to a determined inversion problem of two unknowns, i.e., H_V and z_0 that can be inverted by a single complex observation $\tilde{\gamma}_V(\kappa_z)$. It can

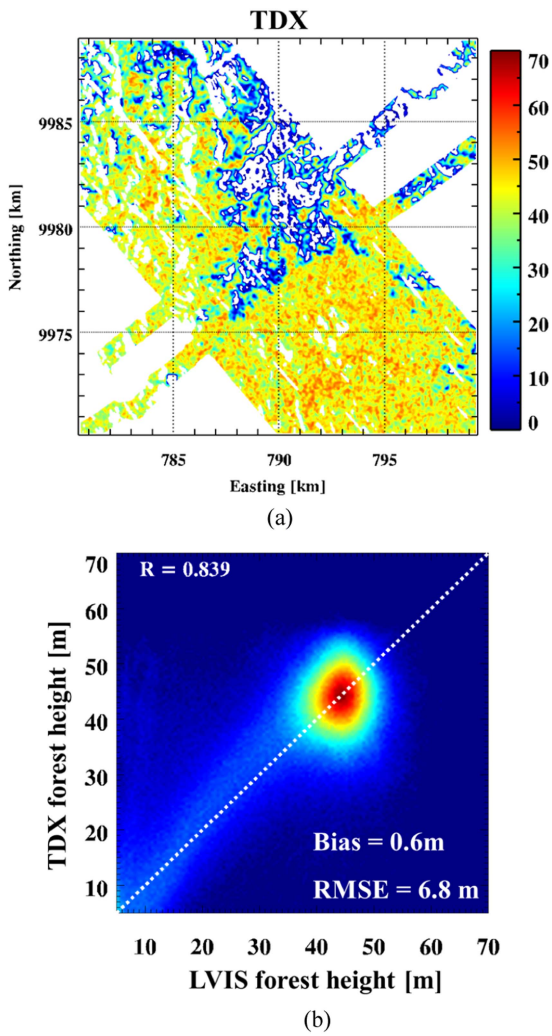

Fig. 7. Lopé site, same area as in Fig. 1. (a) TanDEM-X forest height H_{TX100} in meters (m). (b) Comparison (2D histogram) between H_{TX100} and $H_{LVIS100}$.

be further simplified to a single-dimensional inversion problem (with a single unknown H_V) by accounting only the absolute values of (7).

The forest height inversion was performed using a coherence estimation window of 25 m × 25 m (corresponding to about 150 independent looks), compensating for nonvolumetric decorrelation contributions (γ_{SNR}, γ_{rg}, and γ_Q [46]), deriving the mean profile $P_{mean}(z)$ using all available GEDI waveforms in the scene by means of (11) and using both the volume coherence and the mean profile in (7). Samples with $|\gamma_V(\kappa_z)| < 0.25$ and heights higher than 52 m (i.e., the expected maximum top height for the actual vertical wavenumber) were discarded. In a final step, the available GEDI RH100 heights, H_{GEDI}, were used, as proposed in [25], to compensate any residual global bias affecting the vertical wavenumber—height product $\kappa_z H_V$. The obtained heights were projected in geographic UTM coordinates and resampled in a 20 m grid and are indicated with H_{TX} in the following.

Fig. 5(a)–(b) shows the TanDEM-X height estimates and their validation against the LVIS heights (H_{LVIS}) by means of a 2D histogram. The performance is consistent with what was already reported in [25], confirming the robustness of the inversion with respect to the number of available waveforms. The considerable underestimation of a number of stands with heights above 40 m is partly due to the large vertical wavenumber and partly due to the limited X-band penetration in the dense(r) stands. The underestimation introduced by a too large vertical wavenumber is well known and has been discussed for the actual TanDEM-X / GEDI case in [25].

It is clear that the adapted forest height inversion approach relies on a number of critical assumptions and compromises. The use of a single "mean" vertical reflectivity profile over a whole TanDEM-X scene makes an adaptation to the spatial forest structure heterogeneity. At the same time, there are inherent differences between the nadir lidar waveforms and the side-looking X-band reflectivity. However, such assumptions and compromises are necessary for obtaining forest height from single-pol single-baseline TanDEM-X data. A detailed performance analysis of the implemented forest height inversion can be found in [25].

B. Structure Dependency of the Height Estimation Bias

While the height underestimation due to too large vertical wavenumbers can be avoided by using a smaller spatial baseline, the underestimation due to limited penetration is a fundamental limitation that cannot be easily overcome, if not at all. Nevertheless, a first-order correction is attempted, based on the assumption that even in dense stands there may be points where the X-band pulses penetrate to the ground and allow undistorted height inversion.

To explore this, 25 H_{TX} samples, equivalent to 16 independent estimates with 25 m resolution (see Table I), are aggregated to a height estimate H_{TX100} at 100 m resolution

$$H_{TX100} = \frac{1}{N}\sum_{n=1}^{N} H_{TX}. \tag{12}$$

For sparse stands, the mean of the $N = 25$ H_{TX} height samples is taken, while for dense stands only the mean of the tallest $N = 5$ H_{TX} samples are taken. To discriminate between sparse and dense stands, the horizontal structure index σ_{top} is used.

The effect of this approach is demonstrated using two representative forest areas shown in Fig. 6, a dense one (A) and a sparse(r) one (B) [see Fig. 6(b)], each about 300 m × 300 m. In area (A), the CHM, shown in the top row, varies about 10 m around a mean height of 45 m, indicating a rather dense forest. The estimated H_{TX} heights at 25 m resolution are shown in the second row. From the comparison between the histogram of the estimated heights and that of the RH100 LVIS heights (H_{LVIS}) of the same area an underestimation of about 20 m is evident. Differently, in area (B), the CHM indicates a sparse forest. Here the histograms of H_{TX} and H_{LVIS} are very similar, except for heights lower than 15 m which appear overestimated in H_{TX}. For the rest, the histograms indicate an unbiased inversion performance, supported by a qualitative comparison between the CHM heights and the TanDEM-X heights in the first and second rows, respectively. In the third, fourth, and fifth rows,

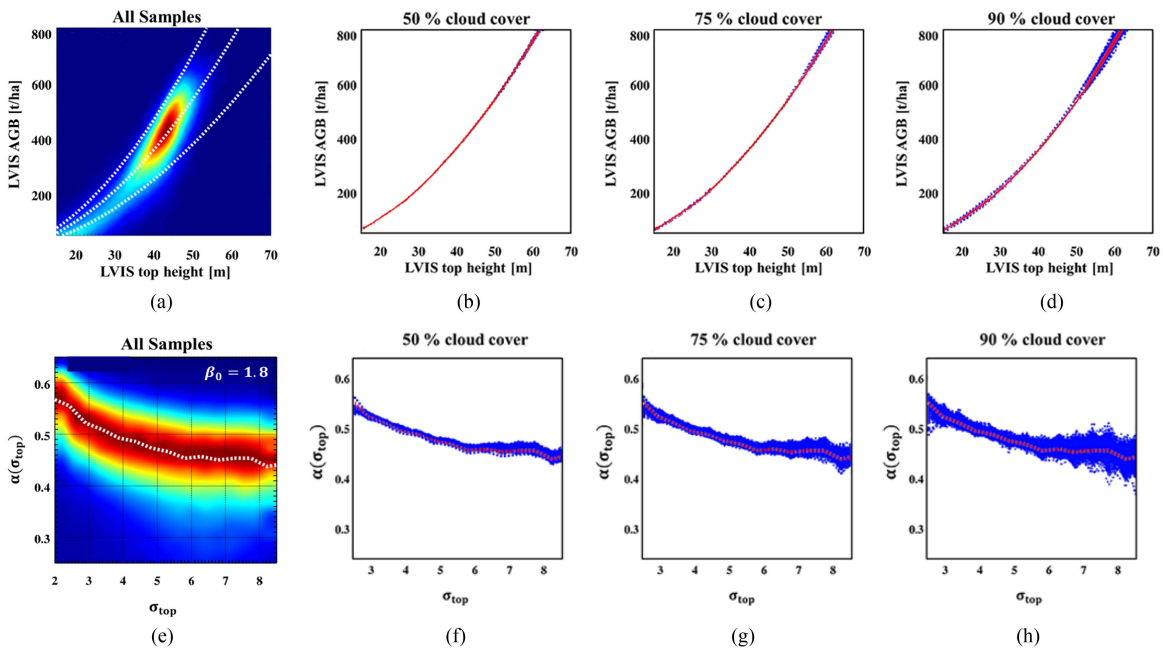

Fig. 8. Lopé site, same area as in Fig. 1. Top row: (a) 2D histogram relating $H_{LVIS100}$ and $B_{LVIS100}$ in correspondence of all the GEDI sampling positions in Fig. 1(b); the central white dashed line represents the height-to-biomass relationship with constant $\alpha = \alpha_0$ obtained using (13), while the upper/lower dashed lines represent the cases in which the fitted α_0 is increased/decreased by the 30%. Panels (b)–(d): the blue dashed lines represent the allometric relationships for $\alpha = \alpha_0$ obtained using (13) in each trial of the simulated 50%, 75%, and 90% cloud covers, respectively. The same relationship obtained in the full-sampling case [as in panel (a)] is reported in red for reference. Bottom row: (e) 2D histogram relating the allometric factor α and σ_{top} using $H_{LVIS100}$, $B_{LVIS100}$ and $\beta_0 = 1.8$ in correspondence with all the GEDI sampling positions in Fig. 1(b) ; the white dashed line represents $\alpha(\sigma_{top})$ obtained using (14). Panels (f)–(h): the blue dashed lines represent the relationships $\alpha(\sigma_{top})$ obtained using (14) in each trial of the simulated 50%, 75%, and 90% cloud covers. The same relationship obtained in the full-sampling case [as in panel (e)] is reported in red for reference.

the aggregated forest height maps [in the sense of (12)] of the two areas and the associated height histograms corresponding to a 100 m resolution (e.g., 100 m $\times$ 100 m) are shown. For the maps shown in the third row, only the tallest of the 25 available height estimates H_{TX} is used, in the fourth row, the mean of the tallest 5 estimates, while in the fifth row, the mean of all 25 height estimates. With respect to $H_{LVIS100}$, comparing the two areas becomes obvious that while using the tallest height estimate compensates for the underestimation in the dense area (A), the sparse area (B) is heavily overestimated. The opposite is the case when using the mean of all estimated heights: in the dense area (A), the 100 m resolution heights still underestimate the reference heights, while in the sparse area (B), the 100 m resolution heights appear unbiased.

The final performance is shown in Fig. 7 in terms of a 2D histogram comparing H_{TX100} and $H_{LVIS100}$. As expected, $N = 5$ corrects the height estimation bias in the tall/dense stands between 40 and 50 m. The residual (positive) bias of around 5 m in this height interval occurs in correspondence with the sparse stands, for which $N = 5$ is not optimal. In contrast, $N = 25$ minimizes the bias in the short(er)/sparse(r) stands. Notice that, in this case, a residual bias between 5 and 10 m persists especially for mean heights between 10 and 20 m and cannot be corrected further by (12). The result does not change significantly when taking the 3 or 7 tallest heights: 5 are selected because they correspond to the H100 metric that refers to the 100 tallest trees in a hectare. As single trees are not seen, the corresponding 20% of height estimates are used. Regarding the σ_{top} threshold for separating between sparse and dense stands, its selection is rather uncritical. Here, a value of 6 m was used. In principle, the threshold has to differentiate between very open and close canopy forest. For a closed canopy forest, the H100 metric applied by using the average of the tallest 5 heights of the 25 samples does not change when the lower heights are underestimated. For open canopy forests, the top canopy height is becoming less and less appropriate with decreasing tree density. In this case, the mean of all heights is more representative.

As a final remark, it was verified that if an optimal N is employed for each cell in the scene, the same conclusion on the residual bias would apply and the RMSE would improve from 6.8 to only 6.3 m. This confirms that the suboptimality of the processing has only minor effects on the final performance.

V. Derivation of Footprint-Level Lidar Allometry

A. Sampling Effect

According to (1), the AGB is an exponential function of top canopy height H with constant allometric exponent β_0 over larger scales. For the case where also the allometric factor α is assumed to be constant over the whole site, the resulting allometric parameters $\alpha = \alpha_0$ and β_0 can be directly derived from the available forest height and AGB measurements, collected in the vectors $\mathbf{h}_{lid}$ and $\mathbf{b}_{lid}$, through a least-squares regression as

$$\min_{\alpha_0,\, \beta_0} \|\mathbf{b}_{lid} - \alpha_0 \mathbf{h}_{lid}^{\beta_0}\|^2. \tag{13}$$

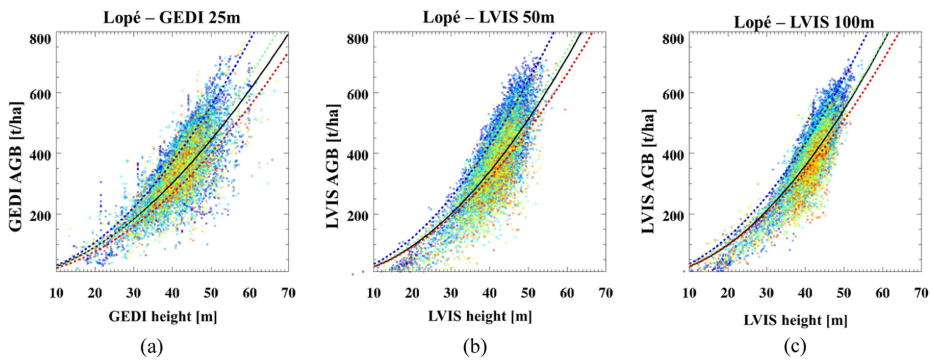

Fig. 9. Lopé site, same area as in Fig. 1. Scatterplots between (a) H_{GEDI} and B_{GEDI}, (b) H_{LVIS50} and B_{LVIS50}, and (c) $H_{LVIS100}$ and $B_{LVIS100}$. The points in the scatterplot correspond to a spatially homogenous subset of the acquired GEDI footprint coverage. The color of each point corresponds to a different value of σ_{top} (expressed in meters) with the same color map as in Fig. 4. The continuous black line represents the height-to-biomass allometry parameterized by $\alpha = \alpha_0$. The dashed colored lines represent the case $\alpha = \alpha(\sigma_{top})$ for three value of σ_{top} (blue: 2 m, green: 5 m, red: 9 m).

The dependence of forest height-biomass allometry on local stand conditions [3], [4], [5], particularly density, can be accounted for by the dependence of the allometric level $\alpha = \alpha(\sigma_{\text{top}})$ on the horizontal structure index. In this sense, (13) can be modified to consider N_α uniformly distributed and nonoverlapping structure intervals centered at $\{\sigma_{\text{top}_i}\}_{i=1}^{N_\alpha}$ in the range of values of σ_{top}. For each of these intervals, the allometric levels $\{\alpha(\sigma_{\text{top}_i})\}_{i=1}^{N_\alpha}$ and a reference allometric exponent β_0 are jointly estimated as

$$\min_{\{\alpha(\sigma_{\text{top}_i})\}_{i=1}^{N_\alpha},\ \beta_0} \left\| \begin{bmatrix} \mathbf{b}_{\text{lid},1} \\ \vdots \\ \mathbf{b}_{\text{lid},i} \\ \vdots \\ \mathbf{b}_{\text{lid},N_\alpha} \end{bmatrix} - \begin{bmatrix} \alpha\left(\text{top}_i\right) \mathbf{h}_{\text{lid},1}^{\beta_0} \\ \vdots \\ \alpha\left(\text{top}_i\right) \mathbf{h}_{\text{lid},i}^{\beta_0} \\ \vdots \\ \alpha\left(\text{top}_{N_\alpha}\right) \mathbf{h}_{\text{lid},N_\alpha}^{\beta_0} \end{bmatrix} \right\|^2 \quad (14)$$

where $\mathbf{b}_{\text{lid},i}$ and $\mathbf{h}_{\text{lid},i}$ are the vectors containing the lidar AGB and height values, respectively, for the generic i-th σ_{top} interval centered at σ_{top_i}.

Accordingly, the height-to-biomass relationship and the dependence of the allometric level $\alpha = \alpha(\sigma_{\text{top}})$ on the horizontal structure index are derived from the available set of forest height and AGB measurements. In all the considered cases, the optimization (14) was carried out using $N_\alpha = 50$ for σ_{top} varying between 0 and 10 m. In the case of GEDI, a more or less sparse (depending on latitude and cloud cover) sampling of forest height and AGB measurements at footprint level is available. In order to evaluate how much the available measurements are sufficient to derive allometric relations, four different scenarios are considered: the full data set scenario using all available LVIS forest height ($H_{LVIS100}$) and AGB ($B_{LVIS100}$) measurements and three thinned scenarios derived by randomly reducing the full LVIS data set along simulated GEDI ground tracks according to three different cloud cover rates (50%, 75%, and 90%). Each of the three thinned scenarios has been generated 200 times (trials), each time by removing a different set of measurements. The number of lidar height and biomass measurements available in each σ_{top} interval varies between 50 and 400 in the full data set, but it can be reduced to around 10 in the most challenging sampling scenario.

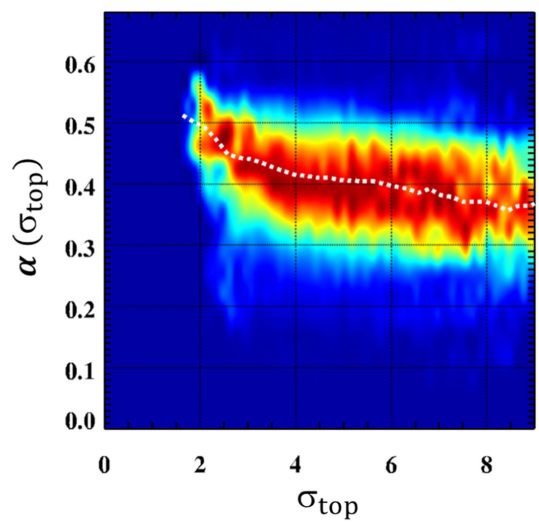

Fig. 10. Lopé site, same area as in Fig. 1. 2D histograms relating α_0 and σ_{top} using H_{GEDI} and B_{GEDI}. The white dashed lines represent the relationship $\alpha(\sigma_{top})$ obtained using (14).

The top row of Fig. 8 shows the obtained allometries derived according to (13) for the case of constant $\alpha = \alpha_0$. In the reference full data set case, the 2D histogram shows the distribution of $B_{LVIS100}$ as a function of $H_{LVIS100}$, while the white dashed lines represent the allometry for the fitted α_0 (central line) and for the cases in which α_0 is increased/decreased by 30%. In the other three plots, the blue dashed lines represent the allometries obtained in each of the 200 trials. The allometric relationship results are very stable with respect to the number of available samples, even in the case where only 10% of the samples are available (e.g., 90% cloud cover).

The bottom row of Fig. 8 shows the obtained allometries derived according to (14) for the case of a variable allometric level $\alpha = \alpha(\sigma_{\text{top}})$. In the reference full data set case, the 2D histograms show the distribution of $\alpha = B_{LVIS100} / H_{LVIS100}^{\beta_0}$ at the sampling locations with $\beta_0 = 1.8$. It is apparent that the

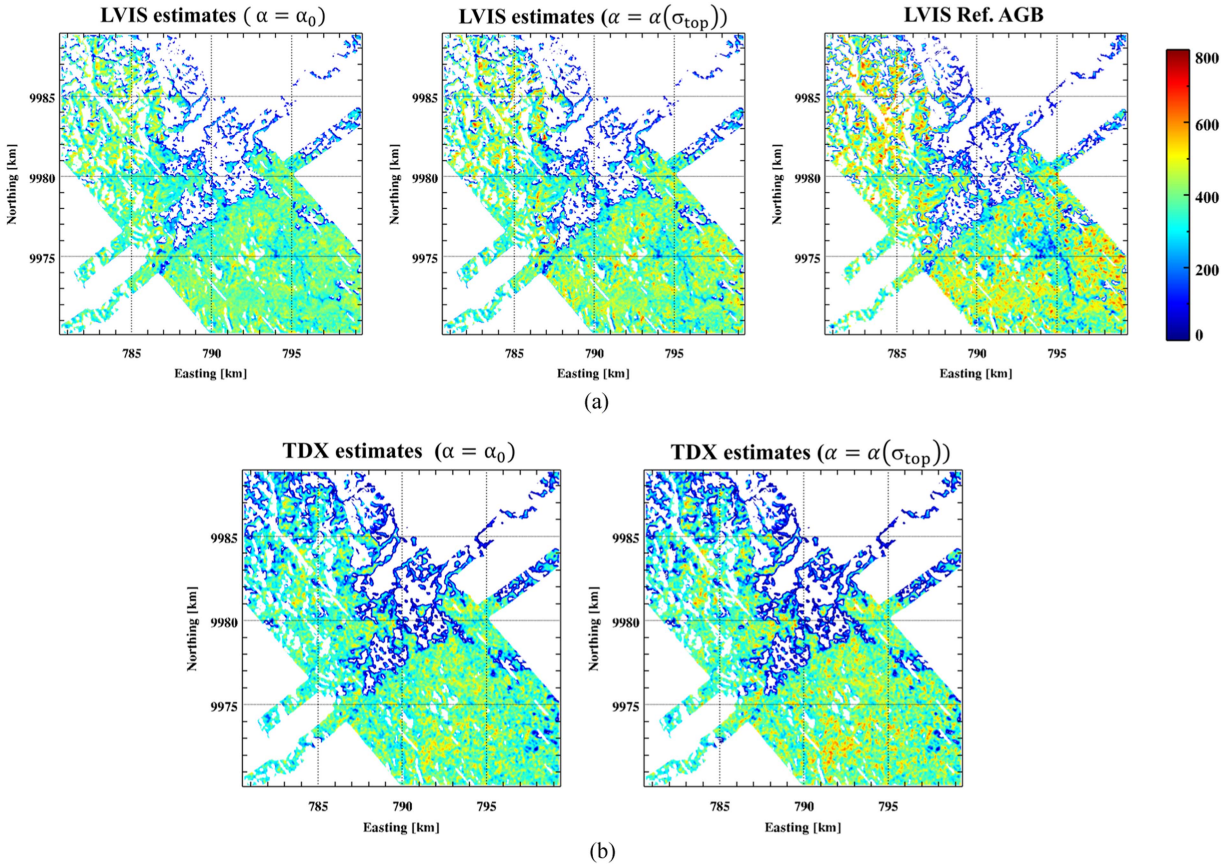

Fig. 11. Lopé site, same area as in Fig. 1. AGB maps obtained from allometric relationships derived using H_{GEDI} and B_{GEDI}, and using (a) $H_{LVIS100}$ with $\alpha = \alpha_0$ (right), $H_{LVIS100}$ with $\alpha = \alpha(\sigma_{top})$ (middle), and reference $B_{LVIS100}$ (left). (b) H_{TX100} with fixed $\alpha = \alpha_0$ (left), and with $\alpha = \alpha(\sigma_{top})$.

obtained allometry is less stable than with $\alpha = \alpha_0$ when the number of available samples decreases because (14) demands more samples to define every allometric parameter in each interval. This is especially true with increasing forest heterogeneity. While for the cases of 50% and 75% of cloud cover $\alpha = \alpha(\sigma_{top})$ can be reconstructed, in the case of 90% cloud cover the $\alpha = \alpha(\sigma_{top})$ relationship cannot be established any longer.

In the case of limited samples, one possible tradeoff is to increase the intervals used to fit the $\alpha = \alpha(\sigma_{top})$ relationship [see (14)] and so doing to reduce their number N_α. In this case, a more robust allometric relationship could be obtained at the cost of a low(er) structure resolution. However, the (real) GEDI samples available over Lopé correspond to almost 50% cloud cover case making the reconstruction of both allometries possible.

B. Scale Effects

After investigating the effect of available samples on the reconstructed allometry, the next question to face concerns the spatial scales on which the allometry is addressed. While GEDI provides measurements (forest height and AGB) at the footprint level of approximately 25 m diameter, the structure index σ_{top} used to refine the allometry is estimated at a 100 m resolution. A lower resolution of σ_{top} would not include a statistically relevant number of CHPs, thus not providing a significant structure description.

In order to investigate the effect of this scale discrepancy on the parameterization of the height-to-biomass relationship, the allometric exponent and the (structure-dependent) allometric level are derived at two different spatial resolutions, 50 and 100 m using the reference LVIS biomass estimates and compared with the ones obtained by using the 25 m GEDI estimates H_{GEDI} and B_{GEDI}. The obtained allometries are shown in Fig. 9. For each resolution, the regression has been performed individually. For the case of a constant allometric coefficient in all three resolutions, a very similar parameterization has been obtained: $\alpha_0 = 0.454$ and $\beta_0 = 1.76$ at 25 m, $\alpha_0 = 0.392$ and $\beta_0 = 1.83$ at 50 m, and $\alpha_0 = 0.383$ and $\beta_0 = 1.85$ at 100 m, respectively.

The color of each point in the scatterplot corresponds to a different value of σ_{top}. As expected, for the same height, the allometric factor decreases with increasing σ_{top} as a consequence of a decrease in (forest) density. This demonstrates the potential of using σ_{top} to adapt the height-to-biomass allometry to the local forest conditions. The adaptation is more effective toward the extremes of the σ_{top} range where the correlation between σ_{top} and the allometric factor is higher. At the 25 m scale, the adaptation appears less effective as σ_{top} appears less correlated to the allometric factor. This can be a result of the large-scale difference between the GEDI samples and σ_{top}. At the same time, the rather low geolocation accuracy of the GEDI footprints of about 10 m at 1 sigma [47] is not supportive.

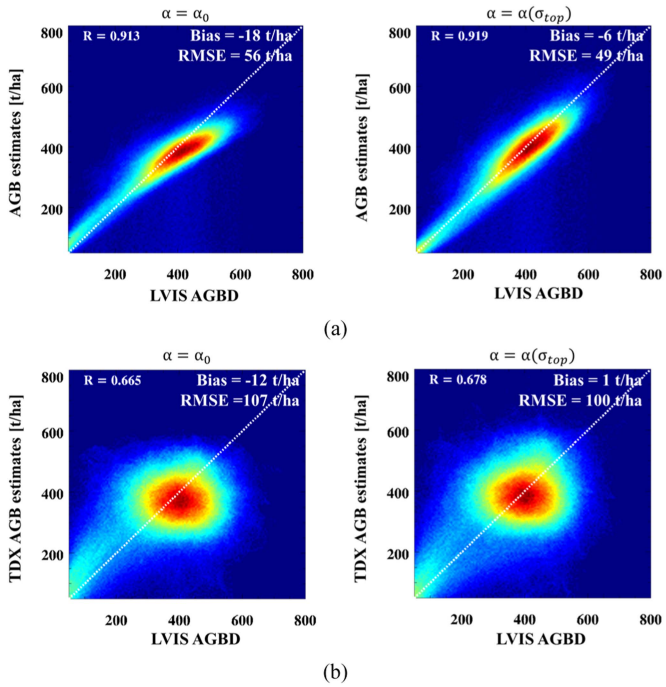

Fig. 12. Comparison (2D histograms) between the reference $B_{LVIS100}$ and the estimated AGB values using (a) $H_{LVIS100}$ and (b) H_{TX100}. In both (a) and (b), $\alpha = \alpha_0$ is used in the left panel, and a variable allometric factor $\alpha = \alpha(\sigma_{top})$ is used in the right panel.

VI. Forest Biomass Estimation and Validation

The performance of the height-to-biomass allometry at 100 m resolution is now addressed by exploring the established dependency of the allometric factor α on the horizontal structure index σ_{top}.

In order to assess the improvement obtained by using the adaptive allometric relation assuming no uncertainty in the forest height, first the LVIS heights $H_{LVIS100}$ are used in the constant (with $\alpha = \alpha_0$) and in the adaptive [with $\alpha = \alpha(\sigma_{top})$] allometric relations derived using H_{GEDI} and B_{GEDI}. In the latter case, the relationship between the allometric factor and σ_{top} is shown in Fig. 10 (white dashed line). The optimization (14) was carried out using $N_\alpha = 50$ for σ_{top} varying between 0 and 10 m. The obtained AGB maps for both cases are shown on the top row (left and middle respectively) of Fig. 11. At the right, the reference $B_{LVIS100}$ derived at 100 m resolution is shown. The validation plots of the obtained AGB maps against the reference AGB are shown on the top row of Fig. 12. The constant $\alpha = \alpha_0$ allometry already provides sensitive results, but the high AGB levels are consistently underestimated and low AGB levels tend to be overestimated. Both effects are compensated when applying the adaptive $\alpha = \alpha(\sigma_{top})$ allometry that provides almost unbiased estimates.

The same procedure is now repeated using instead of the LVIS heights $H_{LVIS100}$ the TanDEM-X heights H_{TX100}. The obtained AG maps are shown on the bottom row of Fig. 11, while the corresponding validation plots are on the bottom row of Fig. 12. The forest height uncertainty dominates the obtained performance. Nevertheless, the adaptive allometry successfully compensates for the overestimation of the lower AGB range as well as the underestimation of the upper AGB range of the constant allometry, allowing for practically unbiased estimates.

VII. Conclusion

The use of the forest height-to-biomass allometry, as addressed in (1), in the context of continuous TanDEM-X InSAR measurements and discrete height and biomass GEDI measurements over a diverse tropical test site, the Lopé National Park in Gabon, is discussed. Important points are the importance of forest structure and the possibility of deriving and using a forest structure index from TanDEM-X data in the absence of a DTM.

Two points are particularly critical to the success of such an approach: 1) the knowledge of the allometric parameters α_0 and β_0 that define the height-to-biomass allometry and their spatial variation in heterogeneous forests; and 2) the ability of TanDEM-X interferometric measurements to provide unbiased forest height estimates in dense forest conditions. In both cases, forest structure and its spatial variability play a decisive role. The proposed methodology illustrates how the sensitivity of the

TanDEM-X interferometric measurements of horizontal forest structure, given by the high spatial resolution and the high attenuation at X-band, can be used to account for the forest heterogeneity and support this way both points.

For this purpose, a horizontal structure index was proposed, similar to the one in [18], but modified to be derived from relative height variations and thus not requiring a DTM. The height variations induced by the topography were compensated by using a low-pass filtered version of the interferogram to access the spatial variations of the top canopy layer. However, as the proposed structural index only takes into account relative height variations, it cannot reliably recognise whether the height changes occur in the upper tree canopy or within the volume. To maximise the sensitivity to the top canopy variations, CHPs are used. The horizontal structure index is then given by the spatial variance of the CHP "top" peaks within a structure cell. Accordingly, a large variance resulting from large canopy height variations is associated with a large canopy roughness and interpreted as "sparse forest." On the other hand, a low variance resulting from low canopy height variations is associated with low canopy roughness and is interpreted as a close canopy, e.g., a "denser forest."

The derived horizontal structure index is used to improve both the forest height estimation and the forest height-to-biomass allometry performance.

The main limitation in forest height estimation is the underestimation of dense stands caused by the limited penetration at X-band that leads to biased (underestimated) heights. Assuming that even in dense stands there may be points where the X-band pulses penetrate to the ground, an unbiased estimation can be attempted at the expense of spatial resolution. For this, the derived horizontal structure index is used to distinguish between "sparse" and "dense" forests: for the "sparse" forest stands a 100 m height estimate is obtained by averaging 25 height estimates at 25 m, for the "dense" forest stands only the mean of the highest 5 estimates is considered.

Looking on the forest height-to-biomass allometry now, the underlying allometry can be derived from the GEDI footprint measurements, i.e., the RH100 heights and the associated AGB values. The simulation of scenarios with different sampling densities shows that the derived underlying allometry is robust to the number of available footprint measurements used to define it, as long as the samples remain representative of forest conditions. This does not appear to be a critical limitation as the underlying allometry, which is primarily dependent on large scale forest attributes (as species composition and the site growth conditions), remains at larger scales. However, this underlying allometry in Lopé underestimates high AGB levels as the spatial forest heterogeneity cannot be represented by a single allometric relation.

The horizontal structure index is here used to adapt the underlying height-to-biomass allometry to the spatial (stand density) heterogeneity for improving biomass estimation performance. This has been attempted by expressing the allometric level as a function of the derived horizontal structure index and using the GEDI footprint measurements, i.e., the RH100 heights, and the associated AGB values to reconstruct this dependency. The obtained monotonous decreasing dependence of the allometric level on the horizontal structural index points to the presence of a real(istic) correlation. This reflects on the achieved biomass estimation performance improvement, when compared to the use of a single allometry. This improvement has been obtained even if the horizontal structure index cannot distinguish vertical variations of density along height. The largest remaining uncertainty contribution in terms of bias and/or variance has been seen to be attributable to the propagation of the height estimation uncertainty.

Even if a single test site has been investigated, the intention of this article is to develop a methodological concept under the perspective of forest biomass inversion on a large scale rather than discussing the optimization of performance on local scales. Nevertheless, the same concept applied within the same test site, but with different acquisition configurations in terms of incidence angles and vertical wavenumber, leads to the same conclusions. Surely, in the future some local optimization may improve the final performance. The extension of this analysis to other test sites is, however, complicated by the availability of large-scale continuous data for validation, especially in terms of biomass.

The results characterize the potential and the limitations of TanDEM-X interferometry for characterizing forest conditions. On the one hand, the high attenuation rates at X-band and the resulting limited penetration into the forest volume maximize the interferometric sensitivity to the spatial variations of the top canopy layer and make it especially appropriate for the characterization of the horizontal forest structure. At the same time, the high spatial resolution of the TanDEM-X interferograms and its continuous measurement nature allows the estimation of forest structure variations at spatial scales relevant for the characterization of the horizontal forest structure. On the other hand, the same limited penetration into the forest volume, which favors the horizontal forest structure characterisation, limits the height estimation performance and makes the characterisation of the vertical forest structure at reasonable scales almost impossible.

Finally, the proposed methodology and the obtained results demonstrate the synergetic potential of the continuous TanDEM-X and the discrete GEDI measurements. This is because both measurements 1) are at the same time similar enough due to the high sensitivity to the geometrical architecture of the canopy and the high spatial resolution common to both configurations, facilitating a common interpretation and) are different enough because of the different acquisition geometries and measurement approaches to carry independent information.

Acknowledgmnet

The LiDAR AfriSAR data sets were provided by the Land, Vegetation and Ice Sensor (LVIS) team in Code 61A at NASA Goddard Space Flight Center with support from the University of Maryland, College Park, Maryland, USA.

References

[1] T. Mette, K. Papathanassiou, I. Hajnsek, H. Pretzsch, and P. Biber, "Applying a common allometric equation to convert forest height from pol-InSAR data to forest biomass," in *Proc. IEEE Int. Geosci. Remote Sens. Symp.*, 2004, pp. 269–272.

[2] G. P. Asner et al., "A universal airborne LiDAR approach for tropical forest carbon mapping," *Oecologia*, vol. 168, no. 4, pp. 1147–1160, Apr. 2012.

[3] T. Mette, K. Papathanassiou, and I. Hajnsek, "Biomass estimation from polarimetric SAR interferometry over heterogeneous forest terrain," in *Proc. IEEE Int. Geosci. Remote Sens. Symp.*, 2004, pp. 511–514.

[4] A. Torano Caicoya, F. Kugler, I. Hajnsek, and K. Papathanassiou, "LargeScale biomass classification in boreal forests with TanDEM-X data," *IEEE Trans. Geosci. Remote Sens.*, vol. 54, no. 10, pp. 5935–5951, Oct. 2016.

[5] N. Knapp, R. Fischer, and A. Huth, "Linking LiDAR and forest modeling to assess biomass estimation across scales and disturbance states," *Remote Sens. Environ.*, vol. 205, Feb. 2020, Art. no. 111597.

[6] G. Krieger et al., "TanDEM-X: A satellite formation for high-resolution SAR interferometry," *IEEE Trans. Geosci. Remote Sens.*, vol. 45, no. 11, pp. 3317–3341, Nov. 2007.

[7] R. Dubayah et al., "The global ecosystem dynamics investigation: High-resolution laser ranging of the earth's forests and topography," *Sci. Remote Sens.*, vol. 1, 2020, Art. no. 100002.

[8] L. Duncanson et al., "Aboveground biomass density models for NASA's global ecosystem dynamics investigation (GEDI) LiDAR mission," *Remote Sens. Environ.*, vol. 270, Mar. 2022, Art. no. 112845.

[9] M. Brolly, M. Simard, H. Tang, R. O. Dubayah, and J. P. Fisk, "A lidar-radar framework to assess the impact of vertical forest structure on interferometric coherence," *IEEE J. Sel. Topics Appl. Earth Observ. Remote Sens.*, vol. 9, no. 12, pp. 5830–5841, Dec. 2016.

[10] E. C. De Grandi, E. Mitchard, and D. Hoekman, "Wavelet based analysis of TanDEM-X and LiDAR DEMs across a tropical vegetation heterogeneity gradient driven by fire disturbance in Indonesia," *Remote Sens.*, vol. 8, no. 8, pp. 641–667, Aug. 2016.

[11] P. Da Conceição Bispo et al., "Mapping forest successional stages in the brazilian amazon using forest heights derived from TanDEM-X SAR interferometry," *Remote Sens. Environ.*, vol. 232, Jul. 2019, Art. no. 111194.

[12] S. Erasmi, M. Semmler, P. Schall, and M. Schlund, "Sensitivity of bistatic TanDEM-X data to stand structural parameters in temperate forests," *Remote Sens.*, vol. 11, Dec. 2019, Art. no. 2966.

[13] J. I. H. Askne, H. J. Persson, and L. M. H. Ulander, "On the sensitivity of TanDEM-X observations to Boreal forest structure," *Remote Sens.*, vol. 11, Dec. 2019, Art. no. 1644.

[14] M. J. Soja, H. J. Persson, and L. M. H. Ulander, "Estimation of forest height and canopy density from a single InSAR correlation coefficient," *IEEE Geosci. Remote Sens. Lett.*, vol. 12, no. 3, pp. 646–650, Dec. 2014.

[15] S. Solberg, E. H. Hansen, T. Gobakken, E. Naessset, and E. Zahabu, "Biomass and InSAR height relationship in a dense tropical forest," *Remote Sens. Environ.*, vol. 192, pp. 166–175, Apr. 2017.

[16] M. Tello Alonso, V. Cazcarra Bes, M. Pardini, and K. Papathanassiou, "Forest structure characterization from SAR tomography at L-band," *IEEE J. Sel. Topics Appl. Earth Observ. Remote Sens.*, vol. 11, no. 10, pp. 3402–3414, Oct. 2018.

[17] V. Cazcarra Bes, M. Tello Alonso, R. Fischer, M. Heym, and K. Papathanassiou, "Monitoring of forest structure dynamics by means of Lband SAR tomography," *Remote Sens.*, vol. 9, no. 12, pp. 1229–1250, Nov. 2017.

[18] C. Choi, M. Pardini, M. Heym, and K. Papathanassiou, "Improving forest height-to-biomass allometry with structure information: A TanDEM-X study," *IEEE J. Sel. Topics Appl. Earth Observ. Remote Sens.*, vol. 14, pp. 10415–10427, Sep. 2021.

[19] L. Reineke, "Perfecting a stand-density index for even aged forests," *J. Agricultural Res.*, vol. 46, no. 7, pp. 627–638, 1933.

[20] H. Chen, S. R. Cloude, D. G. Goodenough, D. A. Hill, and A. Nesdoly, "Radar forest height estimation in mountainous terrain using tandem-X coherence data," *IEEE J. Sel. Top. Appl. Earth Observ. Remote Sens.*, vol. 11, no. 10, pp. 3443–3452, Oct. 2018.

[21] M. Schlund, A. Wenzel, N. Camarretta, C. Stiegler, and S. Erasmi, "Vegetation canopy height estimation in dynamic tropical landscapes with TanDEM-X supported by GEDI data," *Methods Ecol. Evol.*, vol. 14, pp. 1639–1656, 2022.

[22] W. Qi et al., "Improved forest height estimation by fusion of simulated GEDI Lidar data and TanDEM-X InSAR data," *Remote Sens. Environ.*, vol. 221, pp. 621–634, 2019.

[23] Y. Lei, R. Treuhaft, and F. Gonçalves, "Automated estimation of forest height and underlying topography over a Brazilian tropical forest with single-baseline single- polarization TanDEM-X SAR interferometry," *Remote Sens. Environ.*, vol. 252, Jan. 2021, Art. no. 112132.

[24] R. Guliaev, V. Cazcarra-Bes, M. Pardini, and K. Papathanassiou, "Forest height estimation by means of TanDEM-X InSAR and waveform lidar data," *IEEE J. Sel. Top. Appl. Earth Observ. Remote Sens.*, vol. 14, pp. 3084–3094, 2021.

[25] C. Choi et al., "Large-scale forest height mapping by combining TanDEM-X and GEDI data," *IEEE J. Sel. Top. Appl. Earth Observ. Remote Sens.*, vol. 16, pp. 2374–2385, Feb. 2023.

[26] I. Hajnsek et al., "Technical assistance for the development of airborne SAR and geophysical measurements during the AfriSAR campaign," ESA, Tech. Rep. 4000114293/15/NL/CT, 2016. [Online]. Available: https://earth.esa.int/documents/10174/134665/AfriSAR-Final-Report

[27] L. Fatoyinbo et al., "The NASA AfriSAR campaign: Airborne SAR and lidar measurements of tropical forest structure and biomass in support of future space missions," *Remote Sens. Environ.*, vol. 264, Oct. 2021, Art. no. 112533.

[28] J. Armston et al., *AfriSAR: Gridded Forest Biomass and Canopy Metrics Derived from LVIS, Gabon*. Oak Ridge, TN, USA: ORNL DAAC, 2016, doi: 10.3334/ORNLDAAC/1775.

[29] N. Labriere et al., "In situ reference datasets from the TropiSAR and AfriSAR campaigns in support of upcoming spaceborne biomass missions," *IEEE J. Sel. Top. Appl. Earth Observ. Remote Sens.*, vol. 11, no. 10, pp. 3617–3627, Oct. 2018.

[30] S. M. Marselis, H. Tang, J. D. Armston, K. Calders, N. Labrière, and R. Dubayah, "Distinguishing vegetation types with airborne waveform lidardata in a tropical forest-savanna mosaic: A case study in Lopé National Park, Gabon," *Remote Sens. Environ.*, vol. 216, pp. 626–634, Oct. 2018.

[31] E. T. A. Mitchard et al., "Mapping tropical forest biomass with radar and spaceborne LiDAR in Lopé National Park, Gabon: Overcoming problems of high biomass and persistent cloud," *Biogeosciences*, vol. 9, no. 1, pp. 179–191, Jan. 2012.

[32] C. A. Silva et al., "Comparison of small- and large-footprint LiDAR characterization of tropical forest aboveground structure and biomass: A case study from central Gabon," *IEEE J. Sel. Top. Appl. Earth Observ. Remote Sens.*, vol. 11, no. 10, pp. 3512–3526, Oct. 2018.

[33] F. Kugler, S. K. Lee, I. Hajnsek, and K. P. Papathanassiou, "Forest height estimation by means of pol-InSAR data inversion: The role of the vertical wavenumber," *IEEE Trans. Geosci. Remote Sens.*, vol. 53, no. 10, pp. 5294–5311, Oct. 2015.

[34] R. O. Dubayah, M. Hofton, J. B. Blair, J. Armston, H. Tang, and S. Luthcke, *GEDI L2A Elevation and Height Metrics Data Global Footprint Level V001, 2020b. NASA EOSDIS Land Processes DAAC*. Sioux Falls, SD, USA: DAAC, 2020, doi: 10.5067/GEDI/GEDI02A.001.

[35] R. O. Dubayah et al., *GEDI L4A Footprint Level Aboveground Biomass Density, Version 1, 2021*. Oak Ridge, TN, USA: ORNL DAAC, 2021, doi: 10.3334/ORNLDAAC/1907.

[36] R. Treuhaft et al., "Vegetation profiles in tropical forests from multibaseline interferometric synthetic aperture radar, field, and LiDAR measurements," *J. Geophys. Res., Atmospheres*, vol. 114, no. D23, Dec. 2009, Art. no. 250125.

[37] R. Treuhaft et al., "Tropical-forest biomass estimation at X-band from the spaceborne TanDEM-X interferometer," *IEEE Geosci. Remote Sens. Lett.*, vol. 12, no. 2, pp. 239–243, Aug. 2014.

[38] E. C. De Grandi, E. Mitchard, I. H. Woodhouse, and G. D. De Grandi, "Spatial wavelet statistics of SAR backscatter for characterizing degraded forest: A case study from Cameroon," *IEEE J. Sel. Topics Appl. Earth Observ. Remote Sens.*, vol. 8, no. 7, pp. 3572–3584, May 2015.

[39] F. Kugler, D. Schulze, I. Hajnsek, H. Pretzsch, and K. Papathanassiou, "TanDEM-X Pol-InSAR performance for forest height estimation," *IEEE Trans. Geosci. Remote Sens.*, vol. 52, no. 10, pp. 6404–6422, Oct. 2014.

[40] G. D. De Grandi and E. C. De Grandi, *Spatial Analysis for Radar Remote Sensing of Tropical Forests*. Boca Raton, FL, USA: CRC Press, 2021, pp. 104–110.

[41] G. R. Lee, R. Gommers, F. Wasilewski, K. Wohlfahrt, and A. O'Leary, "PyWavelets: A Python package for wavelet analysis," *J. Open Source Softw.*, vol. 4, no. 36, Apr. 2019, Art. no. 1237.

[42] R. Lanari et al., "Generation of digital elevation models by using SIR-C/X-SAR multifrequency two-pass interferometry: The Etna case study," *IEEE Trans. Geosci. Remote Sens.*, vol. 34, no. 5, pp. 1097–1114, Sep. 1996.

[43] G. H. X. Shiroma and M. Lavalle, "Digital terrain, surface, and canopy height models from InSAR backscatter-height histograms," *IEEE Trans. Geosci. Remote Sens.*, vol. 58, no. 6, pp. 3754–3777, Jan. 2020.

[44] C. Choi, M. Pardini, and K. Papathanassiou, "Quantification of horizontal forest structure from high resolution TanDEM-X interferometric coherences," in *Proc. IEEE Int. Geosci. Remote Sens. Symp.*, 2018, pp. 376–379.

[45] M. Martone et al., "The global forest/non-forest map from TanDEM-X interferometric SAR data," *Remote Sens. Environ.*, vol. 205, pp. 352–373, Feb. 2018.

[46] M. Martone, B. Bräutigam, P. Rizzoli, C. Gonzalez, M. Bachmann, and G. Krieger, "Coherence evaluation of TanDEM-X interferometric data," *ISPRS J. Photogram. Remote Sens.*, vol. 73, pp. 21–29, Sep. 2012.

[47] R. O. Dubayah et al., "Global ecosystem dynamics investigation (GEDI) level 02 user guide: Version 2.0," USGS, Tech. Rep. G15PC00012, 2021. [Online]. Available: https://lpdaac.usgs.gov/documents/986/GEDI02_UserGuide_V2.pdf

Changhyun Choi received the B.S. and M.S. degrees in Earth and environmental sciences from Seoul National University, Seoul, South Korea, in 2014 and 2017, respectively. He has been working toward the Ph.D. degree to monitor forest structure by combining X-band SAR interferometry and Lidar with the Information Retrieval Research Group, Microwaves and Radar Institute, Deutsches Zentrum fur Luft- und Raumfahrt (DLR) in Oberpfaffenhofen, Weßling, Germany, since 2017.

His main research interests are in the area of synthetic aperture radar (SAR) signal processing for forest applications, focusing on the retrieval of forest structural parameters from interferometric SAR data.

Matteo Pardini (Member, IEEE) received the Ms.Eng. degree (*summa cum laude*) in telecommunication engineering and the Ph.D. degree in information engineering from the University of Pisa, Pisa, Italy, in 2006 and 2010, respectively.

In January 2010, he joined the Information Retrieval Group, Radar Concepts Department, Microwaves and Radar Institute, Deutsches Zentrum fur Luft- und Raumfahrt (DLR) in Oberpfaffenhofen, Weßling, Germany, as a Research Scientist, after a visiting research period from August to December 2009. In 2017, he was a Visiting Scientist with the Department of Geographical Sciences, University of Maryland, College Park, MD, USA. His research interests include synthetic aperture radar (SAR) tomographic and polarimetric interferometric processing for 3-D bio/geophysical information extraction over natural volumes (forest, agriculture, and ice), SAR mission design, and SAR mission performance analysis.

Dr. Pardini is a Member of DLR.s TanDEM-X and Tandem-L science teams. He was the recipient of the IEEE GRSS IEEE GRSS J-STARS Paper Award in 2019 and the DLR Science Award in 2020.

John Armston received the B.Sc. degree in biology from Macquarie University, Sydney, NSW, Australia, in 2001, and the B.Sc. (Hons.) and Ph.D. degrees in geography from The University of Queensland, Brisbane, QLD, Australia, in 2004 and 2013, respectively.

He was a Remote Sensing Scientist with the Queensland Government. In 2016, he joined the Global Ecosystem Dynamics Investigation Science Team in 2016. His research interests include quantitative measurement and mapping of forest and woodland structure, and the development of validated satellite mapping products over large areas to support government environmental monitoring programs.

Konstantinos P. Papathanassiou (Fellow, IEEE) received the Dipl. Ing. and the Doctorate degrees from the Department of Physics, Technical University of Graz, Graz, Austria, in 1994 and 1999, respectively.

From 1992 to 1994, he was with the Institute for Digital Image Processing (DIBAG), Joanneum Research, Graz. From 1995 to 1999, he was with the Microwaves and Radar Institute (HR), German Aerospace Center (DLR), Oberpfaffenhofen, Germany. From 1999 to 2000, he was an EU Postdoctoral Fellow with Applied Electromagnetics (AEL), St. Andrews, U.K. Since October 2000, he has been a Senior Scientist with the Microwaves and Radar Institute (HR), DLR, leading the Information Retrieval Research Group. He has authored or coauthored more than 60 peer-reviewed articles in international journals and more than 300 contributions in international conferences and workshops. His main research interests include polarimetric and interferometric processing and calibration techniques, polarimetric SAR interferometry, and the quantitative parameter estimation from SAR data, as well as in SAR mission design and SAR mission performance analysis.

Dr. Papathanassiou is a Member of DLR's TanDEM-X and Tandem-L science teams, JAXA's ALOS-PalSAR Cal-Val teams, ESA's BIOMASS Mission Advisory Group, JAXA's Carbon and Kyoto Initiative, and NASA.s GEDI Mission Science Team. He was the recipient of the IEEE GRSS IGARSS Symposium Prize Paper Award in 1998, the Best Paper Award of the European SAR Conference (EUSAR) in 2002, the IEEE GRSS J-STARS Paper Award in 2019, the DLR Science Award in 2002 and 2020, the DLR's Senior Scientist Award in 2011, and the DLR's Otto Lilienthal Award in 2020.